Food Chemistry: X 21 (2024) 101128

Contents lists available at ScienceDirect

Food Chemistry: X

journal homepage: www.sciencedirect.com/journal/food-chemistry-x

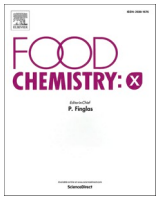

Synthesis, anti-browning effect and mechanism research of kojic acid-coumarin derivatives as anti-tyrosinase inhibitors

Min He [a,b], Jinfeng Zhang [a,b], Na Li [a], Lu Chen [a], Yan He [a], Zhiyun Peng [a,*], Guangcheng Wang [b,*]

[a] Clinical Trails Center, The Affiliated Hospital of Guizhou Medical University, Guiyang, China
[b] State Key Laboratory of Functions and Applications of Medicinal Plants, Guizhou Provincial Key Laboratory of Pharmaceutics, Guizhou Medical University, Guiyang, China

ARTICLE INFO

Keywords:
Coumarin
Kojic acid
TYR inhibitors
Anti-browning

ABSTRACT

Thirteen kojic acid-coumarin derivatives were synthesized using the principle of molecular hybridization, and their structures were characterized by ^{1}H NMR, ^{13}C NMR, and HRMS. *In vitro* enzyme inhibition experiments showed that all newly synthesized derivatives have excellent inhibition of tyrosinase (TYR) activity. As a mixed inhibitor, compound **6f** has the strongest activity, with an IC_{50} value of 0.88 ± 0.10 μM. Multispectral experiments have confirmed that the mode of action of compound **6f** on TYR was static quenching. In addition, compound **6f** formed a new complex with TYR, which increased the hydrophobicity of the enzyme microenvironment, reduced the content of the α-helix in the enzyme, and changed the secondary structure. The experimental results showed that compound **6f** effectively inhibited the browning of lotus root slices and had low cytotoxicity. Therefore, compound **6f** is believed to have great development potential as a TYR inhibitor in the food industry.

1. Introduction

It has been reported that bacteria, fungi, mammals, plants, and humans all possess a unique enzyme that can induce the synthesis of melanin. This enzyme is known as tyrosinase (TYR) in microorganisms, animals, and humans, and is also known as polyphenol oxidase or catechol oxidase in plants. The enzymatic browning reaction is mainly caused by the oxidation of phenolic compounds catalyzed by TYR in fruit and vegetable to form brown substances (Peng et al., 2022). For example, mechanical damage, water loss, and physical damage caused by low temperatures during postharvest storage of fresh fruits and vegetables can activate TYR in cells, leading to browning (Thybo, Christiansen, Kaack, & Petersen, 2006). This will affect the nutrition, flavor, appearance quality, and commodity value of fruits and vegetables, making them difficult to enter the market. Therefore, it is necessary to find efficient and non-toxic TYR inhibitors that directly inhibit TYR to prevent fruit and vegetable browning (Peng et al., 2022).

In the past decades of research, a large number of TYR inhibitors have been isolated and purified from fungi, bacteria, and other microorganisms, the most representative example of which is kojic acid (KA, **1**). However, long-term use has exposed the shortcomings of KA such as poor efficacy, instability, and side effects, which hinders its commercial application (Bentley R., 2006; Burdock et al., 2001). Based on this, a large number of scholars have conducted in-depth research on KA to obtain TYR inhibitors with better activity and safety. For example, (Shao et al., 2018) designed and synthesized six new hydroxypyridinone derivatives, and TYR inhibitors and anti-browning agents with good activity were screened out. In 2022, (Muñoz-Pina et al., 2022) evaluated that small mazamacrocyclic compounds modified with a hydroxypyridinone similar to KA significantly reduced enzymatic browning in fresh apple juice by more than 50 % after stirring for 1 h. A novel KA derivative containing a trolox moiety was synthesized, which exhibited potent TYR inhibitory activity and radical scavenging activity (Ahn et al., 2011).

As is known to all, the structural modification of natural products is an important way to find more active lead compounds. The strategy of skeleton heterozygosity is the key strategy to expand their biological activities, enhance their pharmacological effects and overcome drug resistance. Coumarin is a very important natural product with a benzopyran skeleton. Many studies have shown that coumarin and its derivatives have strong anti-tumor, anti-cancer, anti-oxidation, anti-inflammatory, and TYR inhibition effects (Hussain et al., 2019). Therefore, a class of KA-coumarin analogs was prepared (Fig. 1) and evaluated their TYR inhibitory activity in *in vitro* modes. The anti-

* Corresponding authors.
E-mail addresses: pengzhiyun1986@163.com (Z. Peng), wanggch123@163.com (G. Wang).

https://doi.org/10.1016/j.fochx.2024.101128
Received 3 November 2023; Received in revised form 22 December 2023; Accepted 8 January 2024
Available online 10 January 2024
2590-1575/© 2024 The Author(s). Published by Elsevier Ltd. This is an open access article under the CC BY-NC-ND license (http://creativecommons.org/licenses/by-nc-nd/4.0/).

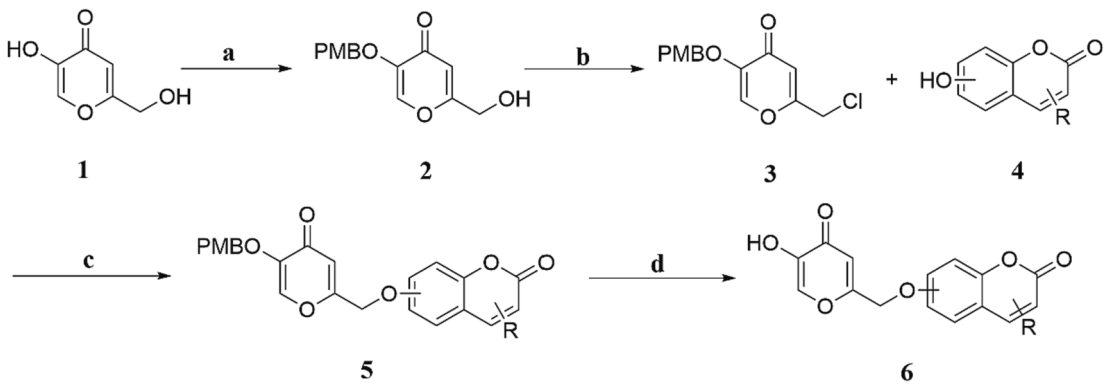

Fig. 1. Synthesis of KA derivatives containing coumarin moiety. (a) 4-Methoxybenzyl chloride, K_2CO_3, DMF, 80 °C, 8 h; (b) Triethylamine, TsCl, CH_2Cl_2, DMAP, r.t, 5 h; (c) K_2CO_3, DMF, 90 °C, 6 h; (d) Trifluoroacetic acid, THF, CH_2Cl_2, r.t, 1 h.

browning effect and mechanism of action on TYR of this series of compounds were also described.

2. Experimental methods

2.1. Chemicals and instruments

TYR and L-DOPA (McLean, Shanghai, China), KA (Aladdin, Shanghai, China), compounds **4a-4c** and **4 k** (Heowns, Tianjin, China), nuclear magnetic resonance spectroscopy (JNM-ECS400, JEOL, Tokyo, Japan), high-resolution mass spectroscopy (UHPLC Q-Exactive Plus Orbitrap HRMS, Thermo Fisher Scientific, Waltham, America), colorimetric spectrophotometer (NR60CP, Threenh, Shenzhen, China), multi-function enzyme marker (Varioskan LUX, Thermo Fisher Scientific, Waltham, America), ultraviolet spectrophotometer (UV-2401PC, Shimadzu, Jiangsu, China), cary eclipse fluorescence spectrophotometer (Xingqiao, Beijing, China), chirascan qCD circular dichroism (Applied Photophysics, Shanghai, China).

2.2. Synthesis of compounds *6a-6 m*

*Synthesis of compound **2***: KA **1** (14.07 mmol), potassium carbonate (16.88 mmol), and 4-methoxybenzyl chloride (15.48 mmol) was dissolved in *N*, *N*-dimethylformamide (20 mL) under magnetic stirring. The resulting solution was kept on refluxing for 8 h at 80 °C. After the reaction is completed, the precipitate diluted with 100 mL water is purified by recrystallization to obtain intermediate **2** (98 %).

*Synthesis of compound **3***: First, 10 mmol intermediate **2** was dissolved in 50 mL dichloromethane and stirred continuously at 0 °C for three minutes. Then, triethylamine (3 mmol), 4-toluenesulfonyl chloride (3 mmol), and 4-dimethylaminopyridine (3 mmol) were sequentially added to the mixed solution and continued to stir at room temperature for 6 h. After the reaction was completed by TLC detection, 200 mL of dichloromethane was added for dilution, and the pH of the mixed solution was adjusted to neutral with 5 % hydrochloric acid. Finally, the collected organic layer solution was combined and dried, and the crude product was purified by silica gel column chromatography (petroleum ether-ethyl acetate = 2:1) to obtain intermediate **3**.

*Synthesis of compounds **4d-j** and **4 l-m***: Compounds **4d-4i** were synthesized with minor modifications following the previous literature (Xie et al., 2008). A mixed solution with 10 mmol appropriate resorcinol, 7.5 mL ethyl-2-methyl-3-oxobutanoate (**4d**, **4 g**) or ethyl 3-oxopentanoate (**4e**, **4f**, and **4 h-i**) and 5 mmol p-toluenesulfonic acid was refluxed at 75 °C for 6 h. Then the mixture was diluted with 10 mL water and recrystallized with methanol to obtain the products **4d-4i**. On the other hand, appropriate 1-(2-hydroxyphenyl)ethan-1-one (1 mmol) and sodium hydride (5 mmol) were mixed into dried toluene (5 mL). The mixed solution was reacted at 0 °C for 30 min and then refluxed at 120 °C for 5 h or until the reaction was completed. An appropriate amount of 10 % HCl was dripped into the obtained reaction solution to adjust the pH of the solution to neutral, and then the resulting precipitate was filtered and dried to obtain the products **4j** and **4 l-m**.

*Intermediates **4a-4c** and **4 k** were obtained through purchase.*

*General experimental for the synthesis of compounds **5a-5 m***: A solution of compound **3** (2 mmol), compound **4** (3 mmol), and potassium carbonate in 10 mL DMF was refluxed at 90 °C for 6 h. After cooling the mixed solution, 30 mL of water was added to produce a large amount of solid precipitation, which was filtered and dried to obtain products **5a-5 m**.

*General experimental for the synthesis of compounds **6a-6 m***: Trifluoroacetic acid (1 mL) was slowly added to 2 mL dichloromethane solution containing compounds **5a-5 m** (1 mmol) and the solution was continuously mixed at 24 °C for 30 min. A large amount of dichloromethane solution was poured into the reaction solution for dilution, and then a saturated sodium bicarbonate solution was used for extraction. Finally, the organic layer was combined and dried, and the final products **6a-6 m** were purified by silica gel column chromatography (petroleum ether-ethyl acetate = 3:1).

2.3. TYR inhibition assay

Using L-DOPA as the substrate and phosphate buffer solution as the blank control, the activity of TYR was determined using an ultraviolet spectrophotometer (UV-2401PC) (Honisch et al., 2022). The substrate L-DOPA (0.5 mM) and TYR solution (200 U/mL) were prepared with phosphate buffer solution (PBS), and the solution of tested compounds or KA was prepared by dissolved in DMSO and diluted with PBS (the final concentration of DMSO < 0.1 %). Before the experiment, 2.9 mL of PBS and 0.1 mL of DMSO were used to deduct the influence of the background solvent. Then, the inhibitor solution (100 μL), the substrate solution (2.8 mL), and the TYR solution (100 μL) were added to a quartz colorimetric dish. After mixing for 1 min, the absorption spectra of the mixed solution were continuously recorded using a UV spectrophotometer (UV-2401PC) at a wavelength of 475 nm within 10 min. Finally, using the inhibitor concentration and enzyme activity inhibition rate as the abscissa and ordinate coordinates, a compound concentration-effect curve can be obtained, and the IC_{50} value of the compound inhibiting tyrosinase can be calculated when the enzyme activity inhibition rate is 50 %. The inhibition rate of compounds on tyrosinase activity is calculated as follows:

$$\text{Relative enzymatic activity}(\%) = A_2/A_1 \times 100\%$$

where A_1 and A_2 are the slopes of the kinetics curves before and after the presence of inhibitors. In this assay, KA was used as the positive control, and the group technical samples of the same biological sample were repeated three times.

2.4. Kinetic analysis of TYR

Based on IC_{50}, the most effective compound **6f** was selected for kinetic analysis. The concentration of TYR was fixed, and compound **6f** (different concentrations) and L-DOPA solutions were successively added to a 3 mL reaction system (pH = 6.8, 0.05 mol/L PBS). The change of product formation amount with time was measured at a wavelength of 475 nm. After the data are obtained, the reciprocal of the residual enzyme activity under the action of inhibitors of different concentrations versus the reciprocal of the substrate concentration was used to plot the Lineweaver-Burk plot. The inhibition type of compound **6f** and enzyme can be determined by comparing the changes in K_m and V_m values, and the inhibition constant value was calculated by using the second derivative equation.

2.5. Copper ions interaction study

TYR is a kind of metalloenzyme with binuclear copper active site, which can catalyze the oxidation of phenol and catechol by the coppers in the presence of oxygen molecule (Ashooriha et al., 2019). Some of the TYR inhibitors have been reported to inhibit the enzyme activity by chelating the copper ion at the activity center of the enzyme, and when small molecule inhibitors with characteristic absorption peaks chelate with copper ions, the absorption peaks show shifts (Shang et al., 2018). Based on this, ultraviolet spectroscopy was used to determine whether the compound **6f** chelates with copper ions. The tested solution of compound **6f** (100 μM) was prepared in methanol. Then, the copper sulfate solution with equal volume and different concentrations was mixed with the compound solution to react at 24 °C for 30 min, and the absorption spectrum between 200 and 600 nm was recorded using an ultraviolet spectrophotometer (UV-2401PC). By analyzing the curves obtained under the action of different copper ion concentrations, it is possible to determine whether the compound interacts with copper ions.

2.6. Fluorescence quenching titration

Referring to the reported method, a fluorescence spectrophotometer (Cary Eclipse) was used to detect the fluorescence intensity of TYR under the action of compound **6f** (Peng et al., 2021). The instrument parameters were set as follows: excitation wavelength: 280 nm, slit width of emission light and excitation light: 5 nm, and detection range of wavelength: 300–450 nm. The interference caused by the absorption peak of the compound to the experiment was eliminated. Then, 2.9 mL of TYR solution (200 U/mL) was poured into the cuvette, and the prepared compound solution (400 μM) was added repeatedly for 10 μL each time (0, 1.37, 2.74, 4.10, 5.44, 6.78, 8.11, 9.43 μM). Finally, the emission spectrum of the mixed solution was repeatedly tested three times. The fluorescence intensity values obtained in the experiment are corrected to avoid being affected by the internal filtering effect of fluorescence (Wang, He, Huang, & Peng, 2023).

By analyzing the data of the fluorescence quenching experiment, it is very important to find out what kind of interaction occurs between the fluorophore and the quenching agent. Therefore, the quenching constant value (K_q), binding constant (K_a), and the number of binding sites (n) were calculated according to the formula reported by Cariola et al. (Cariola, El Chami, Granatieri, & Valgimigli, 2023).

2.7. ANS fluorescence assay

The effect of compound **6f** on the fluorescence intensity of ANS-TYR was measured at an excitation wavelength of 390 nm. The scanning rate of the instrument was set to 600 nm/min, the width of the emission slit was 5 nm, and the emission wavelength was 400–600 nm. First, 90 μL of TYR solution (200 U/mL) and 90 μL of ANS solution (80 μM) were mixed evenly and reacted in the dark at room temperature for 30 min. Second, compound **6f** (600 μM) was gradually added to the mixture by 2.5 μL (0, 8.22, 16.22, 24.00, 31.58, 38.96, 53.16, and 60.00 μM) and recorded. Each experiment was repeated three times to take its average values (Xiong et al., 2019).

2.8. UV spectra measurement

Ultraviolet spectroscopy can be used to reveal the changes in protein structure caused by the interaction between small molecules and proteins and to judge the formation of protein–ligand complexes. By studying the changes in UV absorption of proteins at a wavelength of 280 nm, the structural changes of proteins and the quenching types between proteins and small molecules can be determined. Referring to the reported method, the UV–vis absorption spectra of compound **6f** before and after interaction with TYR were measured (Chen et al., 2021). Based on the IC_{50} value, prepare a concentration of compound **6f** in methanol and dilute to 176 μM with PBS solution. In a 3 mL phosphate buffer system, 300 μL compound **6f** solution and 450 μL TYR solution (200 U/mL, dissolved in PBS) was added to the cuvette. The mixture was thoroughly mixed and incubated for 20 min, and an ultraviolet spectrophotometer (UV-2401PC) was used to measure ultraviolet absorption in the wavelength range from 200 to 600 nm at 3 nm narrow gap. PBS buffer solution was used as blank in order to eliminate background noise, and the control group was PBS with compound **6f** only and PBS system with enzyme only.

2.9. CD spectroscopy

The circular dichroism of tyrosinase in the presence and absence of an inhibitor was obtained by using a CD spectropolarimeter (Chirascan qCD). The instrument parameters are set as follows: optical path: 1 mm, acquisition time: 1 s, scanning wavelength: 2 nm. In a 1 mL buffer solution system, 200 μL of TYR solution (200 U/mL, 1.5625 μM) and different volumes of compound **6f** (15.625 μM) were added. Subsequently, circular dichroism with a concentration ratio of 0:1, 1:1, and 6:1 for **6f**-TYR was recorded in the wavelength range of 200–600 nm. The experimental results were subtracted from the buffer background peak. The content of the secondary structure of TYR was calculated using CDNN software (Xu, Li, Mo, Zou, & Zhao, 2022).

2.10. Molecular modeling analysis

Docking study of compound **6f** with TYR (PDB: 2Y9X) was performed according to the previous report (Forli, Huey, Pique, Sanner, Goodsell, & Olson, 2016; He, Fan, Liu, Li, & Wang, 2021). The crystal structure of TYR was downloaded from a protein database, then the water molecules and ligands are removed, and hydrogen atoms and electric charges are added. The 3D structure of the inhibitor was completed using ChemBio3D Ultra 14.0 software. AutoDockTools 1.5.6 package was used to convert proteins and inhibitors into PDBQT format. In the default protein's PDBQT file, the charge of copper ions is zero, so the charges need to be manually added in the PDBQT file using a text editor (Forli, Huey, Pique, Sanner, Goodsell, & Olson, 2016). For Vina docking, the default parameters were used according to our previous report (He, Fan, Liu, Li, & Wang, 2021). After molecular docking, PyMoL (version 1.7.6) was used to visualize the PDBQT file of inhibitor generated by docking with the PDB format file of TYR downloaded from protein database.

2.11. Anti-browning study

The fresh lotus root without pest and mechanical damage was purchased from the local vegetable market as the research object of browning prevention. First, the soil on the lotus root surface was washed away and cut into thin slices of uniform size. Second, the lotus root slices were treated by soaking in 0.0025 % compound **6f** (W/W, 2.5 mg compound **6f** was dissolved in 100 mL water), 0.0025 % KA (W/W, 2.5 mg KA was dissolved in 100 mL water) or distilled water (control) for 6

Table 1
Inhibitory activity of analogues **6a-6 m** and KA on TYR.

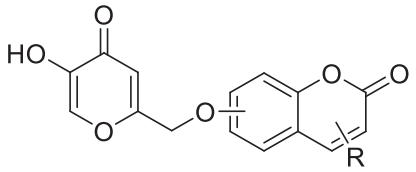

Compound	Substituted position	R	IC_{50} (μM)
6a	7	H	1.62 ± 0.50^{fg}
6b	4	H	5.76 ± 0.57^{d}
6c	7	4-CH_3	1.35 ± 0.52^{fg}
6d	7	3,4,5-$(CH_3)_3$	2.29 ± 0.25^{f}
6e	7	4-CH_2CH_3	0.97 ± 0.10^{g}
6f	7	4-$CH_2CH_2CH_3$	0.89 ± 0.10^{g}
6 g	7	3,4-$(CH_3)_2$	1.51 ± 0.40^{fg}
6 h	7	4,5-$(CH_3)_2$	9.66 ± 0.49^{b}
6i	7	4,8-$(CH_3)_2$	2.23 ± 0.50^{f}
6j	4	6,8-$(CH_3)_2$	8.24 ± 1.69^{c}
6 k	4	7,8-Ph	3.70 ± 1.08^{e}
6 l	4	7-CH_3	5.99 ± 0.18^{d}
6 *m*	4	7-OCH_3	6.68 ± 1.32^{d}
KA			16.38 ± 0.57^{a}

All data have been presented as mean ± SD. a-g, significant differences.

min and drained, and stored aseptically at room temperature. Four indexes were measured within 24 h, and three parallel tests were conducted for each group.

The browning appearance of lotus root slices within 24 h was recorded by a camera, and the surface color properties of different groups of samples were assessed using the (red-green) index of the CIELAB colorimetric system (L*, a*, and b*) (Carcelli et al., 2020). ΔE as an indicator of comprehensive color is obtained by comparing the color with the initial time.

$$\Delta E = \left[(L_t^* - L_{initial}^*)^2 + (a_t^* - a_{initial})^2 + (b_t^* - b_{initial})^2\right]^{0.5}$$

where the L*, a*, and b* indicate lightness, reddish-greenish, and yellowish-bluish, respectively.

2.12. Cellular assays

According to published literature (Li et al., 2022), the CCK-8 was applied to the viability of normal human embryonic kidney cell line HEK-293 in each group (Mocan et al., 2018; Castañeda-Loaiza et al., 2020). The logarithmic phase cells (1×10^5 cells/well) were inoculated into 96-well plates at 37 °C for 24 h, and then treated with solutions of compound **6f** (4, 12, 36, 108 μM) prepared by PBS. After 24 h of interaction with compounds, discarding the mixed solution and washing the 96 well plates twice with PBS, then 0.2 mL of a medium solution containing 10 % CCK-8 was added. After 2 h, the absorbance value of the mixture was recorded with a multi-function enzyme microplate meter (Varioskan Lux) at 450 nm wavelength.

3. Results and discussion

3.1. Chemistry

As recorded in Fig. 1, the hydroxyl group at position 5 of KA **1** was protected with 4-methoxybenzyl chloride, and then it was substituted with 4-toluenesulfonyl chloride under alkaline conditions to obtain intermediate **3**. Under the catalysis of potassium carbonate, compound **3** was reacted with coumarin derivatives to obtain compound **5**, and the protective group is removed from trifluoroacetic acid to obtain the products **6a-6 m** (Fig. S1–S52).

3.2. Inhibitory effect of compounds *6a-6 m* on TYR

In this assay, the concentrations of compounds **6a-6 m** required for 50 % inhibition of TYR (IC_{50}) were evaluated and listed in Table 1. These 13 compounds have significant inhibition on TYR activities, among which compounds **6e** and **6f** have the most prominent activities (IC_{50} = 0.97 ± 0.10 μM, 0.88 ± 0.10 μM, respectively). The structure–activity relationship of KA derivatives was discussed by introducing different substituted coumarins. Compared the inhibitory activity of **6a** (IC_{50} = 1.62 ± 0.50 μM) with **6b** (IC_{50} = 5.76 ± 0.57 μM), the result was shown that the introduction of 7-hydroxycoumarin derivatives in KA showed better anti-TYR activity than that of 4-hydroxycoumarin derivatives.

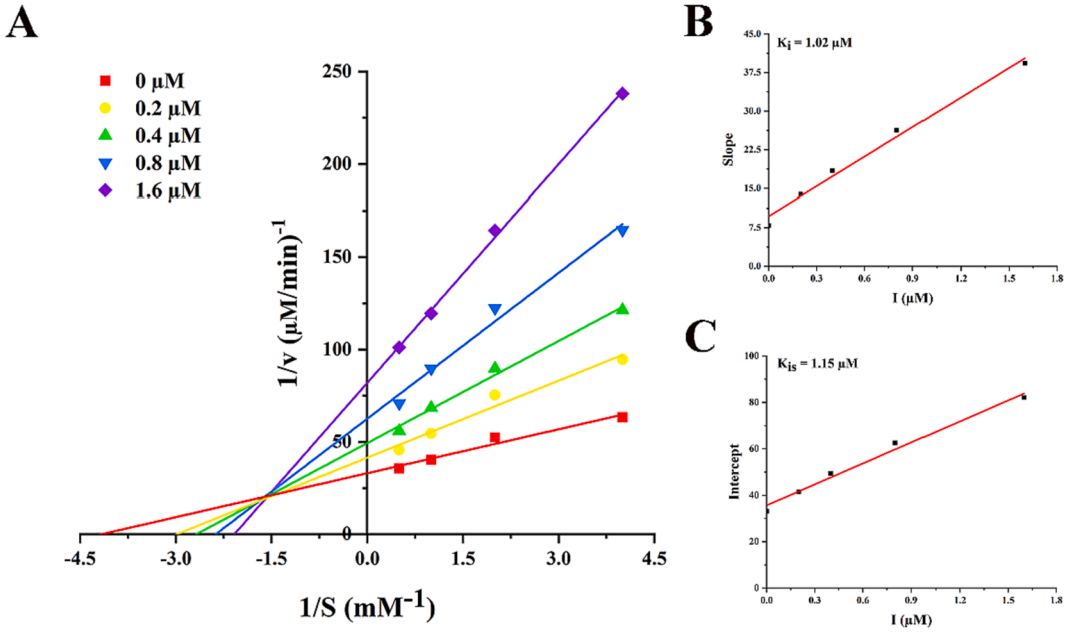

Fig. 2. Determination of the inhibition type and inhibition constant of compound **6f** on TYR. (A) Lineweaver-Burk plot for compound **6f**; (B) The plot of slope versus the concentration of **6f** for determining the inhibition constants K_I. (C)The plot of intercept versus the concentration of inhibitors for determining the inhibition constants K_{IS}.

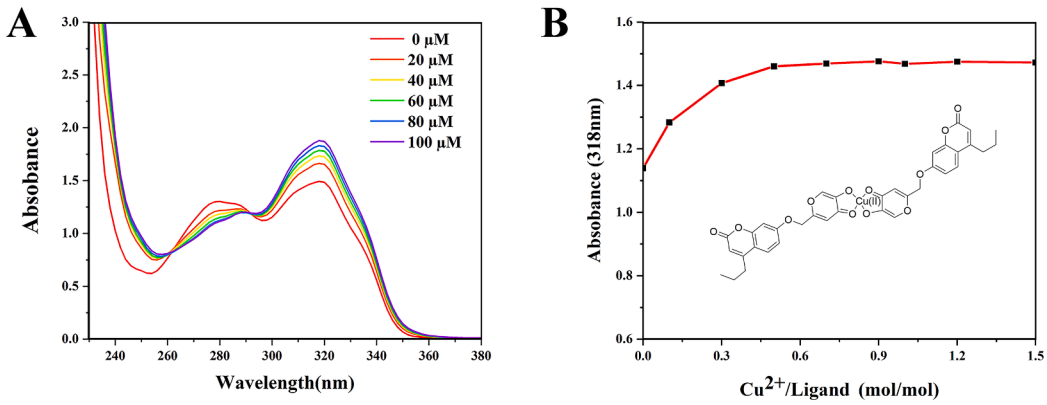

Fig. 3. Copper-chelating activity of compound **6f**. (A) The UV spectrum of compound **6f** (100 μM) alone or with different concentrations of Cu^{2+} (0, 20, 40, 60, 80, and 100 μM) in methanol; (B) The relationship of absorbance and the ratio of Cu^{2+} /ligand.

The possible reason is that the molecular structure of hydroxypyranone at 7-position of coumarin is closer to linear structure than that at position 4, which makes it easy to enter the linear active cavity of TYR (Peng et al., 2021). By comparing the derivatives of coumarin whose 7-hydroxy were replaced by hydroxypyranone (**6a** and **6c-6i**), it was found that the introduction of alkanes can enhance the activity of the compounds, especially the introduction of alkanes at the 4-position. For example, by comparing compounds **6a** (IC_{50} = 1.62 ± 0.50 μM), **6c** (IC_{50} = 1.35 ± 0.52 μM), **6e** (IC_{50} = 0.97 ± 0.10 μM), and **6f** (IC_{50} = 0.88 ± 0.10 μM), it was found that the activity of the compound increases with the extension of the carbon chain. However, the introduction of more substituents at sites other than 4-position leads to reduced activity by comparison compounds **6d** (R = 3,4,5-$(CH_3)_3$), **6 g** (R = 3,4-$(CH_3)_2$), **6 h** (R = 4,5-$(CH_3)_2$) and **6i** (R = 4,8-$(CH_3)_2$) with **6c** (R = 4-CH_3). It may be that the introduction of substituents at these sites increases the steric hindrance of the compound into the linear cavity of TYR, making it unable to bind effectively to the active site, resulting in reduced activity (Raza et al., 2020). On the other hand, by comparing compounds **6b** (IC_{50} = 5.76 ± 0.57 μM), **6 k** (IC_{50} = 3.70 ± 1.08 μM), **6 l** (IC_{50} = 5.99 ± 0.18 μM), and **6 m** (IC_{50} = 6.68 ± 0.32 μM), the introduction of a larger group at 7-position of 4-hydroxycoumarin was more conducive to the inhibition of TYR activity. In order to illustrate the binding interactions of this class of compounds with the active site of TYR, the molecular docking study was performed.

3.3. *Inhibitory kinetics of compound **6f** on TYR*

In the phosphate buffer measuring system with a volume of 3 mL and a concentration of 0.05 mol/L, the enzyme concentration was fixed at 200 U/mL, and then the effects of appropriate concentrations of $_L$-DOPA and inhibitor **6f** on TYR activity were investigated (Chen et al., 2005). With the reciprocal of substrate concentrations as the abscissa and the reciprocal of enzyme reaction rates as the ordinate, a group of straight lines crossing the second quadrant could be obtained. As can be seen from Fig. 2**A**, Lineweaver-Burk plots showed changes in V_{max} (maximum reaction rate) and K_m (Michaelis constant). These characteristics concluded that compound **6f** was an uncompetitive and non-competitive inhibitor, which could bind to both free enzyme and enzyme-substrate complexes (You et al., 2022). The inhibition constant K_I (Fig. 2**B**) of compound **6f** on free enzyme and the K_{IS} (Fig. 2**C**) of compound **6f** on enzyme-substrate complex can be obtained by the quadratic plot of the slope and vertical axis intercept of the linear group on the concentration of inhibitor in Fig. 2**A**. The value of the inhibition constant determines the affinity between the inhibitor and the enzyme, which indicated that the binding ability of compound **6f** to the free enzyme was higher than that of the enzyme-substrate complex, and it was mainly used to inhibit TYR activity by combining with free enzyme (Chai et al., 2018).

3.4. *Copper ions chelation ability of compound **6f** on TYR*

The bottom of the hydrophobic cavity at the active center of TYR contains two divalent copper ions (CuB and CuA) located on the spiral beam, which are highly conservative and essential in the catalytic process of TYR. Using ultraviolet spectroscopy to study the interaction between small molecules with characteristic absorption peaks and copper ions, it is possible to observe whether the characteristic absorption peak of ultraviolet has shifted to determine whether the inhibitor is chelating with copper ions (Shang et al., 2018). The chelation of compound **6f** to copper ions was further investigated using the copper ion titration experiment, and the results are shown in Fig. 3. With the addition of copper ions (0–100 μM), the peak values of the maximum characteristic absorption peaks of compound **6f** gradually decrease and move (Fig. 3**A**). It can be inferred that compound **6f** reduced the catalytic activity of TYR by chelating copper ions on the active site. In addition, the stoichiometric ratio of the **6f**-Cu^{2+} complex can be calculated from Fig. 3**B**. When the concentration of the compound was twice that of copper ion, the absorption curve gradually became flat. It was consistent with the previous research conducted by our laboratory (Wang et al., 2023).

3.5. *Effect of compound **6f** on the fluorescence spectrum of TYR*

Due to the presence of fluorescent chromophores such as tryptophan, tyrosine, and phenylalanine, proteins, and proteases can exhibit endogenous fluorescence properties under excitation. When protease inhibitors interact with protease, they approach the surface or active site of the enzyme, resulting in a decrease in the fluorescence intensity of the protease. Therefore, the fluorescence quenching experiment is an effective method for studying the binding affinity of protease and inhibitor. From **Fig. S53A,** with the increase of the concentration of compound **6f**, the fluorescence intensity of TYR at the maximum emission wavelength gradually decreases, indicating that compound **6f** has a fluorescence quenching effect on TYR (Chai, Yu, Lin, Wei, & Song, 2021). Interestingly, after deducting the self-fluorescence effect of the compound, it can be seen from **Fig. S53A** that the emission wavelength of TYR was also gradually blue-shifted with the addition of compound **6f**. It has been reported that when proteins combine with inhibitors, the enzyme structure will become loose, and the fluorescent chromophore will enter the hydrophilic area from the hydrophobic area, causing changes in the enzyme structure (Asthana et al., 2015). Therefore, the interaction of compound **6f** with TYR has not only affected the microenvironment near the fluorescent group but also changed the hydrophobic environment of amino acid residues subject to fluorescence quenching (Kim et al., 2006).

The results of fluorescence quenching were further analyzed by using

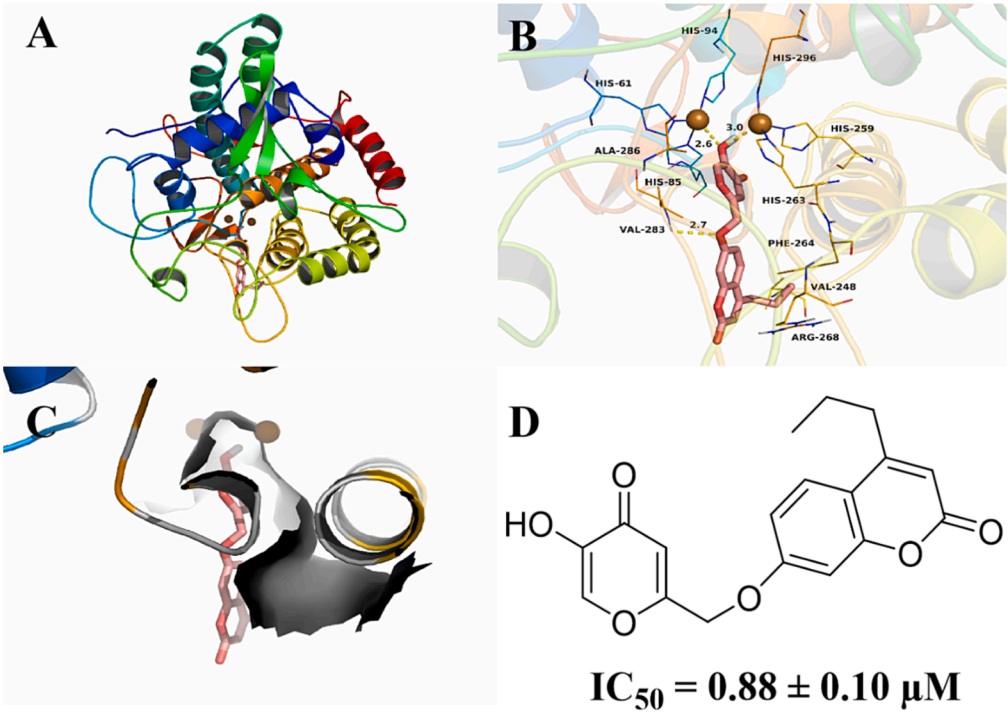

Fig. 4. Docking interaction between **6f** and target protein. (A) Overall structure of tyrosinase with **6f**; (B) Binding pose of **6f** at tropolone binding site; (C) Binding pose of **6f** in the surface of tropolone binding pocket; (D) Chemical Structure of compound **6f**.

the Sterne Volmer plot (Fig. S53**B**). Since the calculated value of K_q was 3.95×10^{12} L/mol S^{-1}, inferring that compound **6f** formed a complex with TYR to inhibit enzyme activity. According to the double reciprocal equation (Fig. S53**C**), $K_A = 2.78 \times 10^4$ L/mol and n = 1.12, indicating that in the absence of a substrate, each TYR protein molecule may have a binding site of compound **6f**.

3.6. Effect of compound *6f* on ANS-TYR fluorescence spectrum

Studying the surface hydrophobicity of proteins is helpful to understand the interactions between proteins and other molecules. ANS is an anionic probe, which can be used to quantitatively characterize the hydrophobicity of protein surface simply and quickly (Xia et al., 2013). In this study, ANS fluorescent dye method was used to detect the interaction between the effector and TYR. As depicted in Fig. S54**A, S54B**, as the concentration of the effector from 0 μM to 60 μM, the maximum emission wavelength of ANS-TYR fluorescence shifted from 533 nm to 500 nm, resulting in a significant blue shift, and the fluorescence intensity continued to increase. The results showed that compound **6f** could alter the enzyme's conformation, exposing the hydrophobic region that binds to ANS (Wang et al., 2019).

3.7. Effect of compound *6f* on the UV spectrum of TYR

The absorbance of the protein at the wavelength of 280 nm is due to the π-π* transition, which reflects the change of tryptophan residue, and the change of the absorption peak at 280 nm indicates that the quenching agent is bound to the protein. Dynamic quenching is mainly caused by the collision and energy transfer between the protein and the quenching agent, and the UV spectrum of the protein does not change during the quenching process. On the contrary, during static quenching, the quenching agent and protein can form a protein-quenching agent complex, which can lead to changes in the ultraviolet spectrum of the protein (Wang et al., 2009; Zhang et al., 2011). Therefore, in order to further clarify the fluorescence quenching mechanism of compound **6f** on TYR, the UV spectroscopy was used to study. The UV absorption spectra of [TYR], [**6f**], [TYR + **6f**], and [(TYR + **6f**) − **6f**], were measured respectively. The experimental results are shown in Fig. S55. The addition of compound **6f** significantly reduced the absorption peak of TYR at 280 nm, indicating that compound **6f** can significantly change the secondary structure of TYR, and the quenching mechanism was consistent with the results of fluorescence spectroscopy experiments (Tao et al., 2022).

3.8. Effect of compound *6f* on circular dichroism of TYR

Circular dichroism (CD) can sensitively monitor the secondary structure changes after the interaction between inhibitors and TYR (He et al., 2016). Fig. S56 has shown the chromatogram of the reaction of compound **6f** with TYR at room temperature at different molar ratio concentrations. As can be seen from Fig. S56, the two negative peaks at 208 nm and 222 nm were typical characteristics of the α-helix structure of TYR (Paudyal et al., 2020). As shown in Table S1, CDNN software was used to calculate the content of each secondary structure of TYR. With the increase of compound **6f** concentration, the content of α-helix decreased (from 34.60 % to 32.50 %), whereas the contents of β-sheet and β-Turn of compound **6f** increased (from 16.50 % to 17.50 %, from 16.80 % to 17.20 %, respectively). These results inferred that the compound **6f** combined with the amino acid residues on the polypeptide chain of TYR and destroy their hydrogen bond network structure. In other words, the complex formed by compound **6f** and TYR induced the secondary structure change of TYR and reduced its stability, thus reducing the catalytic activity of TYR.

3.9. Molecular docking study of compound *6f* with TYR

The interaction between compound **6f** and TYR was studied by molecular simulation. Based on the principle of minimum energy, the molecular docking diagram is shown in Fig. 4. Compound **6f** could enter the hydrophobic cavity of TYR and approach the copper ion active site. The evaluated binding energy between the tyrosinase and **6f** was −8.0 kcal·mol^{-1}. As shown in Fig. 4**A**, compound **6f** has formed a stable

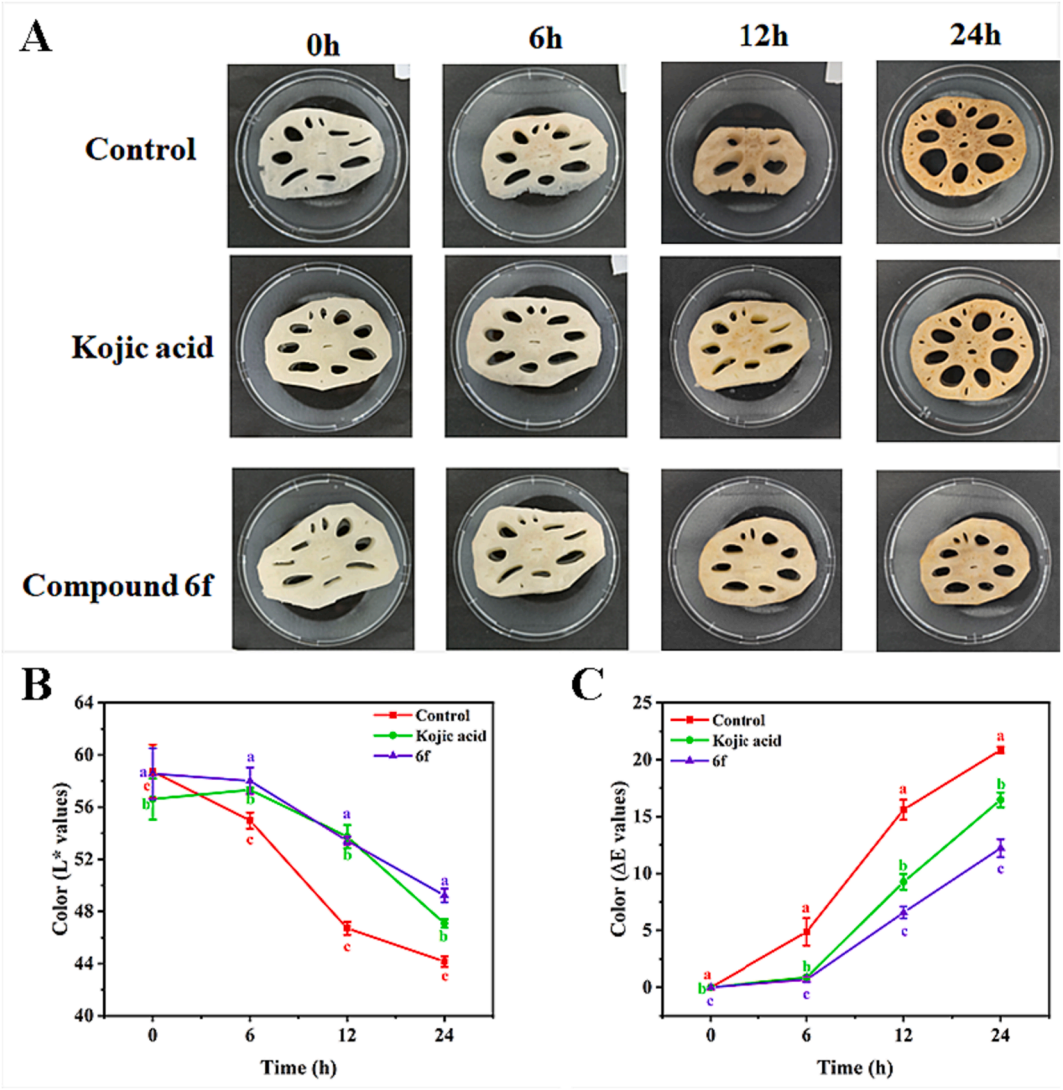

Fig. 5. Browning experiments with slices of fresh-cut lotus root during the 24-storage at rt. (A) Visual appearance of apple slices treated with KA and **6f**; (B) L* value changes; (C) ΔE value changes.

hydrophobic binding with amino acid residues Val-248, Phe-264, Val-283, and Ala-286. There was a hydrogen bond between **6f** and TYR, which increased the strength of noncovalent binding. Interestingly, two key chelating interactions between compound **6f** and copper atoms have been observed, which are the main interactions between compound **6f** and TYR (Fig. 4**B, C**). In addition, π-π stacking was formed between the hydroxypyranone molecule of the compound **6f** and the residue His-263, while the 2H-chromen-2-one group formed a cation-π interaction with the residue Arg-268. It was showed that compound **6f** form a hydrogen bond with the residue Val-283, with the bond length of 2.7 Å. Based on the CD experiment results, it could be inferred that compound **6f** could enter the active center of TYR and noncovalently combine with these amino acid residues. The structure of the TYR active center is changed by hydrophobic force, electrostatic force, and hydrogen bond, resulting in the change of the TYR secondary structure (Zhou et al., 2016).

*3.10. Anti-browning effect of compound **6f** on fresh-cut lotus root slices*

TYR is an important factor leading to the browning of fruit and vegetable systems, and the color difference parameters (L*, a*, b*, and ΔE) were usually used for their browning degree. The L* value refers to the brightness index, representing the degree of browning, with a range of 0–100. Early studies showed that the L* value was more sensitive to browning reaction in lotus root slice systems (Zhang & Ma, 2013). Therefore, L* and ΔE values were used as the main parameters to characterize the anti-browning effect of compound **6f** in lotus root slices. The lotus root slices with uniform size were equally divided into three groups: blank group (water), **6f** group (0.0025 %), and KA group (0.0025 %). In this assay, there was no significant difference in the initial L* value in statistics, and showed a downward trend over time. It could be seen from Fig. 5**B** that the water group has almost no anti-browning effect on lotus root slices at room temperature, while the anti-browning effect of the **6f** group is more obvious than that of the KA group. The browning degree expressed by color difference parameter ΔE was consistent with the L* value (Fig. 5**C**). In addition, the photos also shown that compound **6f** could make lotus root slices stored for 24 h without obvious browning at room temperature (Fig. 5**A**).

*3.11. Toxicity study of compound **6f** on normal cells*

The cytotoxicity of compound **6f** on human normal cell line (HEK-293) was evaluated. The results were summarized in **Table S2**, which indicated that the concentration of compound **6f** from 4 μM to 108 μM showed low toxicity and the cell viability was more than 80 %. Therefore, compound **6f** was considered to be safe in effective concentrations as a potential TYR inhibitor in the food industry.

4. Conclusion

In this study, thirteen KA-coumarin derivatives (**6a-6 m**) were designed and synthesized, and a large number of studies were carried out on them by referring to many literatures. First, the TYR activity inhibition experiment proved that all the synthesized compounds showed excellent activity, especially compound **6f** with the IC_{50} value of 2.52 ± 0.11 μM, which was ten times more active than KA. Then, the kinetic mechanism of the interaction of the most effective compound **6f** with TYR was studied. The results indicated that compound **6f** showed a mixed-type inhibitor with a K_I value of 3.54 μM, which could bind to both the enzyme directly and the enzyme-substrate complex. In order to better understand the interaction mechanism between this series of compounds and TYR, a large number of assays have been carried out, such as fluorescence quenching, copper ion chelation, ultraviolet spectroscopy, molecular docking experiments, etc. These studies concluded that compound **6f** can reduce the activity of the enzyme mainly by chelating with binuclear ketone ions of TYR and changing the hydrophobic environment of the amino acid residues, which affects the secondary structure of the enzyme. Moreover, compound **6f** not only effectively delayed the browning of lotus root slices stored at room temperature for 24 h, but also showed good safety for HEK-293 cells. All in all, we have prepared a class of KA-coumarin derivatives based on the principle of molecular hybridization, which has the potential to be used as TYR inhibitors with anti-browning effects and applied in the food industry.

Funding

This work was supported by National Natural Science Foundation (NSFC) Cultivation project of Affiliated Hospital of Guizhou Medical University (gyfynsfc[2023]-04), China.

CRediT authorship contribution statement

Min He: Data curation, Formal analysis, Investigation, Methodology, Writing – original draft. **Jinfeng Zhang:** Data curation, Investigation, Software. **Na Li:** Software. **Lu Chen:** Resources. **Yan He:** Resources. **Zhiyun Peng:** Funding acquisition, Methodology, Supervision, Writing – review & editing. **Guangcheng Wang:** Methodology, Supervision, Writing – review & editing.

Declaration of competing interest

The authors declare that they have no known competing financial interests or personal relationships that could have appeared to influence the work reported in this paper.

Data availability

The data that has been used is confidential.

Appendix A. Supplementary data

Supplementary data to this article can be found online at https://doi.org/10.1016/j.fochx.2024.101128.

References

Ahn, S. M., Rho, H. S., Baek, H. S., Joo, Y. H., Hong, Y. D., Shin, S. S., & Park, S. N. (2011). Inhibitory activity of novel kojic acid derivative containing trolox moiety on melanogenesis. *Bioorganic & Medicinal Chemistry Letters, 21*(24), 7466–7469. https://doi.org/10.1016/j.bmcl.2011.09.122

Ashooriha, M., Khoshneviszadeh, M., Khoshneviszadeh, M., Moradi, S. E., Rafiei, A., Kardan, M., & Emami, S. (2019). 1,2,3-Triazole-based kojic acid analogs as potent tyrosinase inhibitors: Design, synthesis and biological evaluation. *Bioorganic Chemistry, 82*, 414–422. https://doi.org/10.1016/j.bioorg.2018.10.069

Asthana, S., Zucca, P., Vargiu, A. V., Sanjust, E., Ruggerone, P., & Rescigno, A. (2015). Structure-Activity Relationship Study of Hydroxycoumarins and Mushroom Tyrosinase. *Journal of Agricultural and Food Chemistry, 63*(32), 7236–7244. https://doi.org/10.1021/acs.jafc.5b02636

Bentley, R. (2006). From *miso*, *saké* and *shoyu* to cosmetics: A century of science for kojic acid. *Natural Product Reports, 23*(6), 1046. https://doi.org/10.1039/b603758p

Burdock, G. A., Soni, M. G., & Carabin, I. G. (2001). Evaluation of Health Aspects of Kojic Acid in Food. *Regulatory Toxicology and Pharmacology, 33*(1), 80–101. https://doi.org/10.1006/rtph.2000.1442

Carcelli, M., Rogolino, D., Bartoli, J., Pala, N., Compari, C., Ronda, N., & Fisicaro, E. (2020). Hydroxyphenyl thiosemicarbazones as inhibitors of mushroom tyrosinase and antibrowning agents. *Food Chemistry, 303*, Article 125310. https://doi.org/10.1016/j.foodchem.2019.125310

Cariola, A., El Chami, M., Granatieri, J., & Valgimigli, L. (2023). Anti-tyrosinase and antioxidant activity of meroterpene bakuchiol from Psoralea corylifolia (L.). *Food Chemistry, 405*(Pt B), Article 134953. https://doi.org/10.1016/j.foodchem.2022.134953

Castañeda-Loaiza, V., Placines, C., Rodrigues, M. J., Pereira, C. G., Zengin, G., Neng, N. R., & Custódio, L. (2020). In vitro enzyme inhibitory and anti-oxidant properties, cytotoxicity and chemical composition of the halophyte Malcolmia littorea (L.) R.Br. (Brassicaceae). *Natural Product Research, 35*(22), 4753–4756. https://doi.org/10.1080/14786419.2020.1719484

Chai, W. M., Huang, Q., Lin, M. Z., Ou-Yang, C., Huang, W. Y., Wang, Y. X., & Feng, H. L. (2018). Condensed Tannins from Longan Bark as Inhibitor of Tyrosinase: Structure, Activity, and Mechanism. *Journal of Agricultural and Food Chemistry, 66*(4), 908–917. https://doi.org/10.1021/acs.jafc.7b05481

Chai, W. M., Yu, Z. Y., Lin, M. Z., Wei, Q. M., & Song, S. (2021). 5-Methoxy-2-mercaptobenzimidazole as an efficient inhibitor on tyrosinase: Inhibitory activity and mechanism. *Journal of Bioscience and Bioengineering, 131*(4), 356–363. https://doi.org/10.1016/j.jbiosc.2020.11.009

Chen, Q.-X., Song, K.-K., Qiu, L., Liu, X.-D., Huang, H., & Guo, H.-Y. (2005). Inhibitory effects on mushroom tyrosinase by p-alkoxybenzoic acids. *Food Chemistry, 91*(2), 269–274. https://doi.org/10.1016/j.foodchem.2004.01.078

Chen, R., Shi, Y., Liu, G., Tao, Y., Fan, Y., Wang, X., & Li, L. (2021). Spectroscopic studies and molecular docking on the interaction of delphinidin-3-O-galactoside with tyrosinase. *Biotechnology and Applied Biochemistry, 69*(4), 1327–1338. https://doi.org/10.1002/bab.2205

Forli, S., Huey, R., Pique, M. E., Sanner, M. F., Goodsell, D. S., & Olson, A. J. (2016). Computational protein-ligand docking and virtual drug screening with the AutoDock suite. *Nature Protocols, 11*(5), 905–919. https://doi.org/10.1038/nprot.2016.051

He, J., Wu, D., Zhai, Y., Wang, Q., Ma, X., Yang, H., & Li, H. (2016). Interaction of inosine with human serum albumin as determined by NMR relaxation data and fluorescence methodology. *Journal of Molecular Liquids, 219*, 547–553. https://doi.org/10.1016/j.molliq.2016.03.067

He, M., Fan, M., Liu, W., Li, Y., & Wang, G. (2021). Design, synthesis, molecular modeling, and biological evaluation of novel kojic acid derivatives containing bioactive heterocycle moiety as inhibitors of tyrosinase and antibrowning agents. *Food Chemistry, 362*, Article 130241. https://doi.org/10.1016/j.foodchem.2021.130241

Honisch, C., Gazziero, M., Dallocchio, R., Dessi, A., Fabbri, D., Dettori, M. A., & Ruzza, P. (2022). Antamanide Analogs as Potential Inhibitors of Tyrosinase. *International Journal of Molecular Sciences, 23*(11), 6240. https://doi.org/10.3390/ijms23116240

Hussain, M. I., Syed, Q. A., Khattak, M. N. K., Hafez, B., Reigosa, M. J., & El-Keblawy, A. (2019). Natural product coumarins: Biological and pharmacological perspectives. *Biologia, 74*(7), 863–888. https://doi.org/10.2478/s11756-019-00242-x

Kim, T. Y., & a. Y. J.. (2007). Piceatannol Inhibits Melanogenesis by Its Antioxidative Actions. *Biological & Pharmaceutical Bulletin, 30*(11), 2007–2011. https://doi.org/10.1248/bpb.30.2007

Li, H., Xue, S., Zhang, X., Li, F., Bei, S., & Feng, L. (2022). CircRNA PVT1 modulated cell migration and invasion through Epithelial-Mesenchymal Transition (EMT) mediation in gastric cancer through miR-423-5p/Smad3 pathway. *Regenerative Therapy, 21*, 25–33. https://doi.org/10.1016/j.reth.2022.02.003

Mocan, A., Moldovan, C., Zengin, G., Bender, O., Locatelli, M., Simirgiotis, M., & Crișan, G. (2018). UHPLC-QTOF-MS analysis of bioactive constituents from two Romanian Goji (Lycium barbarum L.) berries cultivars and their antioxidant, enzyme inhibitory, and real-time cytotoxicological evaluation. *Food and Chemical Toxicology, 115*, 414–424. https://doi.org/10.1016/j.fct.2018.01.054

Muñoz-Pina, S., Duch-Calabuig, A., Ros-Lis, J. V., Verdejo, B., García-España, E., Argüelles, Á., & Andrés, A. (2022). A tetraazahydroxypyridinone derivative as inhibitor of apple juice enzymatic browning and oxidation. *LWT - Food Science and Technology, 154*, Article 112778. https://doi.org/10.1016/j.lwt.2021.112778

Paudyal, S., Sharma, S. K., da Silva, R., Mintz, K. J., Liyanage, P. Y., Al-Youbi, A. O., & Leblanc, R. M. (2020). Tyrosinase enzyme Langmuir monolayer: Surface chemistry and spectroscopic study. *Journal of Colloid and Interface Science, 564*, 254–263. https://doi.org/10.1016/j.jcis.2019.12.118

Peng, Z., Wang, G., Zeng, Q., Li, Y., Liu, H., Wang, J., & Zhao, Y. (2022). A systematic review of synthetic tyrosinase inhibitors and their structure-activity relationship. *Critical Reviews in Food Science and Nutrition, 62*(15), 4053–4094. https://doi.org/10.1080/10408398.2021.1871724

Peng, Z., Wang, G., Zeng, Q., Li, Y., Wu, Y., Liu, H., Wang, J., & Zhao, Y. (2021). Synthesis, antioxidant and anti-tyrosinase activity of 1,2,4-triazole hydrazones as antibrowning agents. *Food Chemistry, 341*, Article 128265. https://doi.org/10.1016/j.foodchem.2020.128265

Raza, H., Abbasi, M. A., Azizur, R., Siddiqui, S. Z., Hassan, M., Shah, S. A. A., Shahid, M., Hong, H., & Seo, S. Y. (2020). Design, synthesis and computational studies of N-(substituted-phenyl)-4-(4-phenyl-1-piperazinyl)butanamides as potent anti-

melanogenic and tyrosinase inhibitors. *Journal of Molecular Structure, 1210*, Article 127969. https://doi.org/10.1016/j.molstruc.2020.127969

Shang, C., Zhang, Y., You, X., Guo, N., Wang, Y., Fan, Y., & Liu, W. (2018). The effect of 7,8,4 -trihydroxyflavone on tyrosinase activity and conformation: Spectroscopy and docking studies. *Luminescence, 33*(4), 681–691. https://doi.org/10.1002/bio.3464

Shao, L. L., Wang, X. L., Chen, K., Dong, X. W., Kong, L. M., Zhao, D. Y., & Zhou, T. (2018). Novel hydroxypyridinone derivatives containing an oxime ether moiety: Synthesis, inhibition on mushroom tyrosinase and application in anti-browning of fresh-cut apples. *Food Chemistry, 242*, 174–181. https://doi.org/10.1016/j.foodchem.2017.09.054

Tao, Y., Chen, R., Fan, Y., Liu, G., Wang, M., Wang, S., & Li, L. (2022). Interaction mechanism of pelargonidin against tyrosinase by multi-spectroscopy and molecular docking. *Journal of Molecular Recognition, 35*(6), e2955. https://doi.org/10.1002/jmr.2955

Thybo, A. K., Christiansen, J., Kaack, K., & Petersen, M. A. (2006). Effect of cultivars, wound healing and storage on sensory quality and chemical components in pre-peeled potatoes. *LWT - Food Science and Technology, 39*(2), 166–176. https://doi.org/10.1016/j.lwt.2004.11.010

Wang, G., He, M., Huang, Y., & Peng, Z. (2023). Synthesis and biological evaluation of new kojic acid-1,3,4-oxadiazole hybrids as tyrosinase inhibitors and their application in the anti-browning of fresh-cut mushrooms. *Food Chemistry, 409*, Article 135275. https://doi.org/10.1016/j.foodchem.2022.135275

Wang, Y. Q., Zhang, H. M., & Zhou, Q. H. (2009). Studies on the interaction of caffeine with bovine hemoglobin. *European Journal of Medicinal Chemistry, 44*(5), 2100–2105. https://doi.org/10.1016/j.ejmech.2008.10.010

Wang, Y.-X., Su, W.-C., Wang, Q., Lin, Y.-F., Zhou, Y., Lin, L.-F., & Shi, Y. (2019). Antityrosinase and antioxidant activities of guanidine compounds and effect of guanylthiourea on melanogenesis. *Process Biochemistry, 85*, 84–96. https://doi.org/10.1016/j.procbio.2019.07.003

Xia, Y., Ji, S., Park, J. S., Park, I., Khoi, P. N., Lee, J., & Jung, Y. D. (2013). Inactivation and conformational changes in methyl parathion hydrolase in 2,2,2-trifluoroethanol solutions: Inactivation kinetics and molecular dynamics simulation. *Process Biochemistry, 48*(4), 625–632. https://doi.org/10.1016/j.procbio.2013.02.031

Xie, L., Guo, H.-F., Lu, H., Zhuang, X.-M., Zhang, A.-M., Wu, G., Ruan, J.-X., Zhou, T., Yu, D., Qian, K., Lee, K.-H., & Jiang, S. (2008). Development and Preclinical Studies of Broad-Spectrum Anti-HIV Agent (3'R,4'R)-3-Cyanomethyl-4-methyl-3',4'-di-O-(S)-camphanoyl-(+)-cis-khellactone (3-Cyanomethyl-4-methyl-DCK). *Journal of Medicinal Chemistry, 51*(24), 7689–7696. https://doi.org/10.1021/jm8003009

Xiong, S. L., Lim, G. T., Yin, S. J., Lee, J., Si, Y. X., Yang, J. M., & Qian, G. Y. (2019). The inhibitory effect of pyrogallol on tyrosinase activity and structure: Integration study of inhibition kinetics with molecular dynamics simulation. *International Journal of Biological Macromolecules, 121*, 463–471. https://doi.org/10.1016/j.ijbiomac.2018.10.046

Xu, H., Li, X., Mo, L., Zou, Y., & Zhao, G. (2022). Tyrosinase inhibitory mechanism and the anti-browning properties of piceid and its ester. *Food Chemistry, 390*, Article 133207. https://doi.org/10.1016/j.foodchem.2022.133207

You, Z., Li, Y., Chen, M., Wong, V. K. W., Zhang, K., Zheng, X., & Liu, W. (2022). Inhibition of plant essential oils and their interaction in binary combinations against tyrosinase. *Food & Nutrition Research, 66*, 8466. https://doi.org/10.29219/fnr.v66.8466

Zhang, H. M., Xu, Y. Q., Zhou, Q. H., & Wang, Y. Q. (2011). Investigation of the interaction between chlorophenols and lysozyme in solution. *Journal of Photochemistry and Photobiology B: Biology, 104*(3), 405–413. https://doi.org/10.1016/j.jphotobiol.2011.04.008

Zhang, G., & Ma, Y. (2013). Mechanistic and conformational studies on the interaction of food dye amaranth with human serum albumin by multispectroscopic methods. *Food Chemistry, 136*(2), 442–449. https://doi.org/10.1016/j.foodchem.2012.09.026

Zhou, L., Liu, W., Xiong, Z., Zou, L., Chen, J., Liu, J., & Zhong, J. (2016). Different modes of inhibition for organic acids on polyphenoloxidase. *Food Chemistry, 199*, 439–446. https://doi.org/10.1016/j.foodchem.2015.12.034